Landslides (2005) 2:43–51
DOI 10.1007/s10346-004-0042-0
Received: 16 August 2004
Accepted: 20 December 2004
Published online: 10 February 2005

Oliver Korup

Distribution of landslides in southwest New Zealand

Abstract This study examines the size distribution of a regional medium-scale inventory of 778 landslides in the mountainous southwest of New Zealand. The spatial density of mapped landslides per unit area can be expressed as a negative power–law function of Landslide area A_L spanning three orders of magnitude ($\sim 10^{-2}$–10^{1} km^2). Although observed in other studies on landslide inventories, this relationship is surprising, given the lack of absolute ages, and thus uncertainty about the temporal observation window encompassed by the data. Large slope failures (arbitrarily defined here as having a total affected area A_L>1 km^2) constitute 83% of the total affected landslide area A_{LT}. This dominance by area affects slope morphology, where large-scale landsliding reduces slope angles below the regional modal value of hillslopes, $\varphi_{mod} \sim 39°$. More numerous smaller and shallower failures tend to be superimposed on the pre-existing relief. Empirical scaling relationships show that large landslides involve >10^6 m^3 of material. The volumes V_L of individual preserved and presumably prehistoric (i.e. pre-1840) landslide deposits equate to 10^{0}–10^{2} years of total sediment production from shallow landsliding in the respective catchments, and up to 10^3 years of contemporary regional sediment yield from the mountain ranges. Their presence in an erosional landscape indicates the geomorphic importance of landslides as temporary local sediment storage.

Keywords Landslide inventory · Magnitude and frequency · Landslide volume · Sediment production · New Zealand

Introduction

Landslide inventories are becoming increasingly popular as a platform for quantitative hazard and risk assessment. Linking them to Geographic Information Systems (GIS) allows rapid request-based visualization of slope-failure history of a given region, modelling of predisposing factors, triggering mechanisms, runout, or interference with the drainage network. Several analyses of landslide inventories have stressed functional relationships between landslide magnitude such as affected area or volume, and frequency, either spatial or spatio-temporal (Hovius et al. 1997; Dai and Lee 2001; Guzzetti et al. 2002). Malamud et al. (2004) tested over 300 statistical distributions and suggested a three-parameter inverse gamma function for modelling more-or-less complete inventories derived from regional landsliding-triggering events, i.e. landsliding episodes. Their model can be used to predict spatio-temporal landslide occurrence, e.g. as required in quantitative landslide hazard analysis. Statistically, it also allows the reconstruction of missing data in incomplete distributions.

The typically observed power–law trend in landslide magnitude–frequency relationships (Malamud et al. 2004) however raises the question of its universal applicability, particularly to the larger end-members, i.e. the "tail" of a given distribution. In regional-scale mapping, the distribution of landslide number versus landslide area tends to be skewed in favour of larger landslides, since very small landslides are less likely to be detected by regional mapping methodologies.

This study examines the landslide size distribution of a new inventory of n=778 landslides in mountainous terrain of southwest New Zealand. The key objective is to discuss the significance and geomorphic implications of a power–law trend for large landslides (defined here as affecting a planform area A_L>1 km^2), which were previously sparsely documented in the region, in this distribution. This contribution is intended as a preliminary overview of our understanding of large-scale slope instability in this remote area. It also partly responds to a recent natural hazards report for West Coast Regional Council, which highlighted the need for a comprehensive landslide inventory as a first-priority means for developing a regional landslide knowledge-base (DTEC Consulting Ltd. 2002).

Study area

Slope instability in southwest New Zealand is closely related to the regional tectonic geomorphology, associated with the 800-km-long Alpine Fault, marking the Australian/Pacific plate boundary through South Island, New Zealand (Fig. 1a). The study area comprises the westward-draining catchments of the Southern Alps between the Main Divide and the Alpine Fault, and the Fiordland Mountains, which are additionally drained east- and southward. Active dextral transpression along the onshore portion of the fault causes rapid uplift of the Southern Alps at <10 mm/year (Norris and Cooper 2000). Offshore to the west of Fiordland plate motion is characterized by oblique subduction of the Australian plate (Claypool et al. 2002). Active seismotectonics subject the area to episodic high-magnitude earthquakes (e.g. Wells et al. 1999). In the Southern Alps, the rock is metamorphosed greywacke comprising the Mesozoic Haast Schist Group. High-grade, almost gneissic, schist occurs immediately east of the Alpine Fault, but metamorphic grade decreases progressively to the east, and in places near the Main Divide, low-grade semischist or schistose greywacke occur. The Fiordland Mountains are composed of crystalline Palaeozoic–Mesozoic basement including granites, diorites, gabbros, and orthogneisses of high rock-mass strength. Late Quaternary uplift in southern Fiordland approaches 0.5 mm/year (Kim and Sutherland 2004), although it is possible that uplift is higher in central and northern Fiordland.

The western Southern Alps and Fiordland are characterized by rugged mountain relief with jagged peaks, serrated ridges, and deeply incised valleys. Both regions were extensively glaciated during the Last Glacial Maximum (LGM, ~20,000 year B.P.). Peaks along the Southern Alps Main Divide are typically higher than 2,500 m, reaching a maximum of 3,400 m, and generally decrease southwestwards to 2,000–2,400 m near the Hollyford

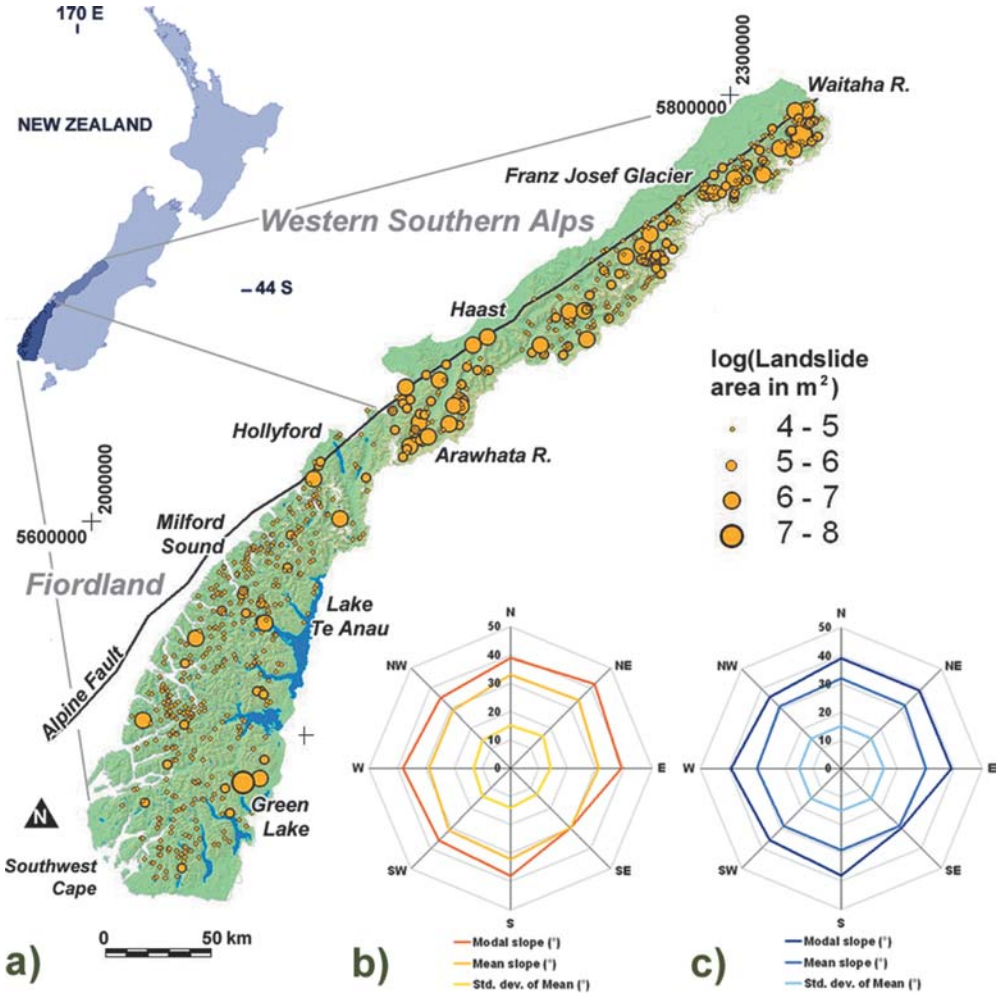

Fig. 1 **a** Study region comprising the western Southern Alps and Fiordland, showing distribution of n=778 mapped landslides. *Inset* shows distribution of modal and mean hillslope angles (incl. standard deviation) as a function of slope aspect classes in **b** South Westland, and **c** Fiordland

valley (Fig. 1a). Elevations at the foot of the range along the Alpine Fault range between 100 and 500 m.

The Fiordland Mountains have a maximum height of 2,000–2,700 m at their northern margin near the Hollyford valley, but elsewhere typically attain 1,400–1,800 m. Relict LGM topography with ice-sculpted slopes and extremely steep-sided U-shaped valleys are well preserved in Fiordland due to very hard rock lithology. Much of the LGM glacial landforms in the comparatively weak schists of the Southern Alps has been extensively modified by post-glacial fluvial dissection (Augustinus 1992). Hillslope angles do not change significantly with slope aspect, although SE-facing slopes tend to be less steep (Fig. 1b and c). The modal slope throughout is ~39°, and on a regional scale shows no influence by the contrast in lithology between the Southern Alps and Fiordland (Fig. 2a and b). The western margin of the Southern Alps receives precipitation of >5 m/year, and <15 m/year west of the Main Divide (Henderson and Thompson 1999). Milford Sound on the western margin of Fiordland receives similar amounts of precipitation, which, although orographically enhanced, does not strongly correlate to local elevation (Wratt et al. 2000).

At present, there are only very small scattered glaciers in Fiordland, compared to more extensive modern glaciation in the Southern Alps, which covers ~11%, and is mainly concentrated southeast of Franz Josef Township (Fig. 1a). Sediment yields are an order of magnitude higher (10^4 t/km^2/year) in the western Southern Alps (Hicks et al. 2003). Thick indigenous rainforests dominated by either conifer/broadleaf species or by southern beech are prolific, covering 40 and 60% of the western Southern Alps and Fiordland, respectively (Mark 1998).

The main predisposing factors for landsliding in southwest New Zealand include reduced rock-mass strength due to earthquake shaking, slope debuttressing by deglaciation and river-incision processes, gravitational stress, and slope dilatation following precursory landsliding. Several reports on landslides in the region suggest that high-intensity rainstorms, fluvial undercutting, and seismic ground shaking are among the most probable trigger mechanisms (Perrin and Hancox 1992; Thomson 1994; Hancox and Perrin 1994; Hancox et al. 1999, 2003; Korup and Crozier 2002; Korup 2004).

Methods

The locations and geomorphometric characteristics of the landslides mapped were obtained from

1. air photo interpretation (API) of over 3000 black-and-white images (mainly 1:50000 scale) from the 1930s to 2002;
2. digital land-cover data (Terralink Ltd 2000), the digital NZMS260 TopoMap (Land Information New Zealand 2002),

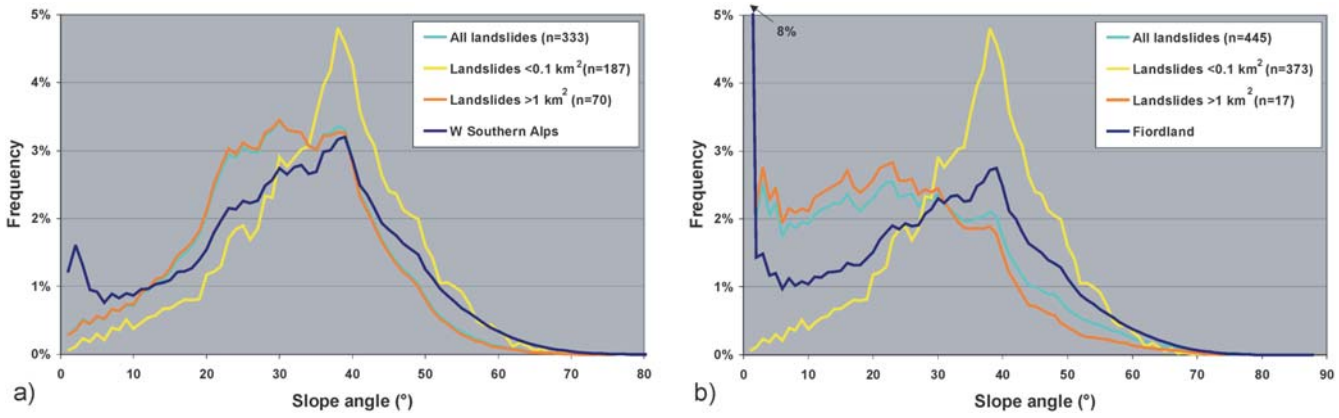

Fig. 2 Frequency distributions of surface-slope angles normalized by area and stratified by landslide area A_L in **a** the western Southern Alps, and **b** Fiordland. *Dark blue curves* show slope-angle distribution of hillslopes, respectively

Table 1 Selected historic landslides in the western Southern Alps and Fiordland

Location	Catchment	Date	Landslide type	Volume (10^6 m^3)	Area (km^2)	Height H (km)	Runout L (km)	Reference
Mt Allen	Waitaha	1900s	Debris flow	>1	3.3	0.9	2.4	Korup (2004)
Gaunt Creek	Waitangitaona	1918	Complex rock/ debris slide, gully erosion	>6.6	0.3	0.4	0.6	Korup et al. (2004); Korup (2005)
Carls Ridge	Wanganui	Post-1930s	Complex rock-block slide	8	0.8	0.8	1.1	Korup and Crozier (2002)
Beelzebub Glacier	Adams	Post-1965	Rock avalanche	1.5	0.2	0.2	0.9	Korup (2005)
Upper Callery	Callery	Post-1965	Debris flow	N/a	0.3	0.9	1.5	This study (Fig. 3)
MacIntosh Creek	Arawhata	Post-1965	Debris flow	0.7	0.7	1.1	2.1	This study
Hirere, Milford Track	Clinton	1982	Rock/debris slide	0.05	0.2	0.9	1.3	This study
Big Slip, Kepler Track	Iris Burn	1984	Rock avalanche	0.3	0.9	0.4	2.0	Thomson (1994)
Undercite Creek	Fox	Jan 1994	Rock/debris slide	1–1.3	N/a	N/a	N/a	DTEC Consulting Ltd (2002)
Mt Adams	Poerua	6 Oct 1999	Rock avalanche	10–15	1.6	1.8	2.8	Hancox et al. (1999)

N/a = not available

including shaded relief images derived from a 25-m grid cell DEM; and

3. review of scientific studies, geological-map descriptions, file reports, university theses, newspaper clippings, and a landslide database on landslides of volumes >10^5 m^3, currently being compiled at the Institute of Geological and Nuclear Sciences, Lower Hutt, New Zealand.

Most historic landslides and associated off-site effects such as erosion or aggradation up- and downstream of failure sites were identified with API on the basis of highly reflective patches in the dense vegetation cover. Brardinoni et al. (2003) outlined various pitfalls of mapping landslides in heavily forested mountain terrain. They noted significant error bars and frequency underestimates resulting from API, when compared to detailed field studies. Similar limits to detection pertain to the subalpine zone of the study area, where the potential of mistaking patches of snow or ice, snow-avalanche chutes, or low-order ravines for landslide scars, resulted in undersampling of actual slope instability.

Coalescing or superimposed landslides were mapped separately, where possible (Fig. 3). Small-scale rock falls, although evident on numerous scree and talus slopes, were excluded from the mapping. Larger and usually fully overgrown failures were detected and mapped on DEM-derived shaded relief images of varying illumination angles and slope-angle overlays (Fig. 4). Postulated large landslides were subsequently investigated in air-photo detail with a 2× mirror stereoscope. Diagnostic landforms included bare headscarps, hummocky and asymmetric deposits, flow lobes, transverse furrows, distinctively uniform vegetation stands, lack of fluvial dissection, and geomorphic impacts on river channels. As opposed to fresh landslide scars and deposits mapped from air photos, most of the larger landslides are completely vegetated and allow no reliable estimate of their age. This excludes larger failures, which were historically documented or which could be temporally bracketed with API (Table 1).

Due to reservations about photogrammetric distortion in alpine relief, n=100 landslides in selected test catchments were repeatedly mapped by the author on independent GIS layers to quantify the accuracy of replication. The resulting maximum

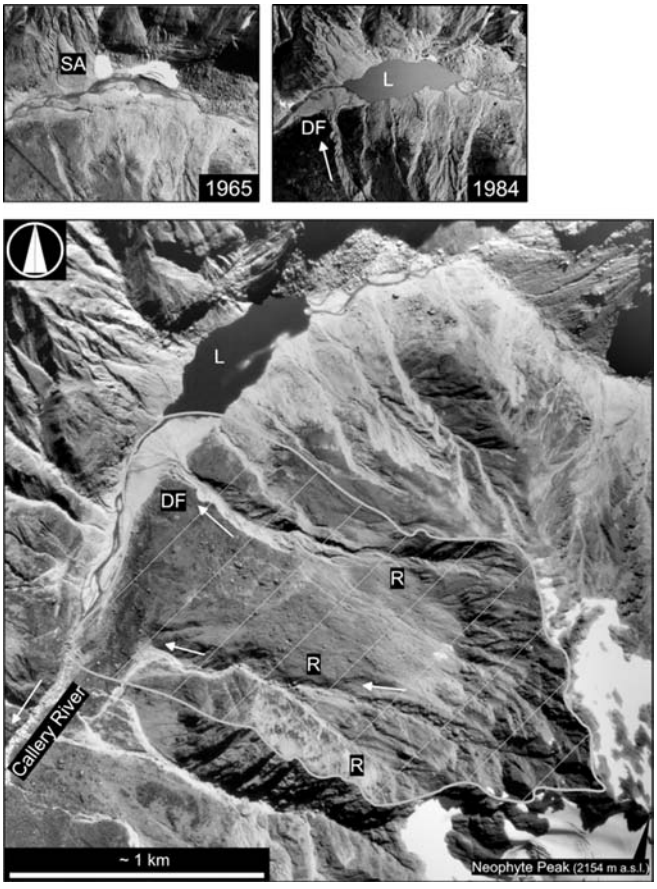

Fig. 3 Ephemeral lake (*L*) dammed by post-1965 debris flows (*DF*) emerging from perched ravines (*R*) exploiting larger deep-seated landslide (>0.7 km^2; *hatched area*), Callery River, western Southern Alps (Table 1). Note talus cones from rock fall/snow avalanching (*SA*). Images courtesy of Land Information New Zealand (1965: SN3722/28; 1984: SNC8340/E2; lower image: SN8478/E16)

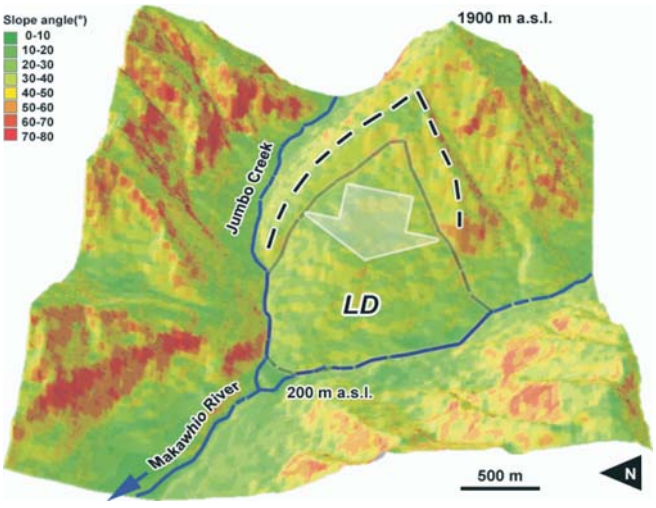

Fig. 4 Slope-angle map draped over shaded digital elevation model (25-m grid) of deep-seated rock flow ("sackung", Cruden and Varnes 1996), confluence of Jumbo Creek and Makawhio River, western Southern Alps. Failure on a schistosity plane extends over ~3 km^2 of the hillslope, and involves ~240×10^6 m^3, forming a characteristically bulging and low-gradient slope (*LD*). *Dashed line* indicates failure scarp

relative error (MRE) in total landslide-affected area was ±10% about the mean (standard error SE=0.5%). Landslide areas obtained from API underestimated the NZMS260 TopoMap extent by 8.5% on average (SE=4.8%). The image distortion in alpine relief was found to be unacceptable and necessitated an integrative mapping protocol. Landslides were postulated from API, and subsequently compared with and mapped directly on the NZMS260 or the corresponding DEM at 1:50000 scale (Fig. 5). A conservative mean relative error for landslide area A_L<30% was assumed. The data obtained are therefore considered to be largely of regional reconnaissance scale and quality.

Landslide inventory

Although there is no comprehensive landslide inventory covering southwest New Zealand as yet, there are presently two major data sets. Hovius et al. (1997) mapped nearly 5000 landslides in montane forests of the western Southern Alps from air photos dating between 1948 and 1987. In a recent study, Hancox et al. (2003) mapped 422 landslides ranging in volume V_L between 10^3 and 10^6 m^3, which were triggered by a M_w=7.2 earthquake near Secretary Island, Fiordland, on 22 August 2003.

The medium-scale (1:50000) inventory described here complements these studies and covers a mountainous area of 18,672 km^2 of southwest New Zealand. The database represented by the inventory is incomplete, and future detection of landslides of all sizes (including large failures) is likely. The cumulative area affected by all mapped landslides A_{LT} is 452 km^2, i.e. 2% of the study area. The database features 846 landslides, of which 778 were digitised as polygons comprising scarp and deposit areas (Fig. 6). The remaining 68 locations, where landslides could not be delineated with confidence, include several very large (V_L>10^8 m^3) failures in Fiordland, which were briefly mentioned by Perrin and Hancox (1992) and Hancox et al. (2003). Although hummocky deposits are evident in most of the mentioned locations, heavily forested terrain and possible obliteration of features by erosion or backfilling did not allow any reliable mapping.

Landslides were arbitrarily labelled "large" when their total affected (planform) area A_L, including scarp and deposit, exceeded 1 km^2. This threshold is partly based on the finding that the substantial inventory of Hovius et al. (1997) used this size as an upper boundary for their investigation. At least 87 failures (10% of the total) in the study area have A_L>1 km^2. There are few data on the depth of failure planes for the landslides. Displaced volumes V_L of large landslides were in n=23 cases estimated by extrapolating contours across well-defined failure scarps or detachment planes (Korup et al. 2004). V_L [km^3] shows a power–law correlation with A_L [km^2], with a slope β=1.95, and intercept k=0.02 (R^2=90%). This empirical relationship predicts a minimum volume of 20×10^6 m^3 for a large landslide. Since the 1999 Mt Adams rock avalanche, which affected ~1.8 km^2, mobilized only 10–15×10^6 m^3 (Hancox et al. 1999), the scaling relationship may be of use for deep-seated failures only. Another volume–area scaling relationship for, however mostly shallow, landslides in South Westland by Hovius et al. (1997) states that a minimum A_L between 0.06 and 0.2 km^2 would be required for a landslide volume V_L > 10^6 m^3.

The range in landslide area for the total sample spans three orders of magnitude from 5×10^{-2} to 5×10^1 km^2 (Figs. 7a and 8a). The frequency density of landsliding, expressed in number of

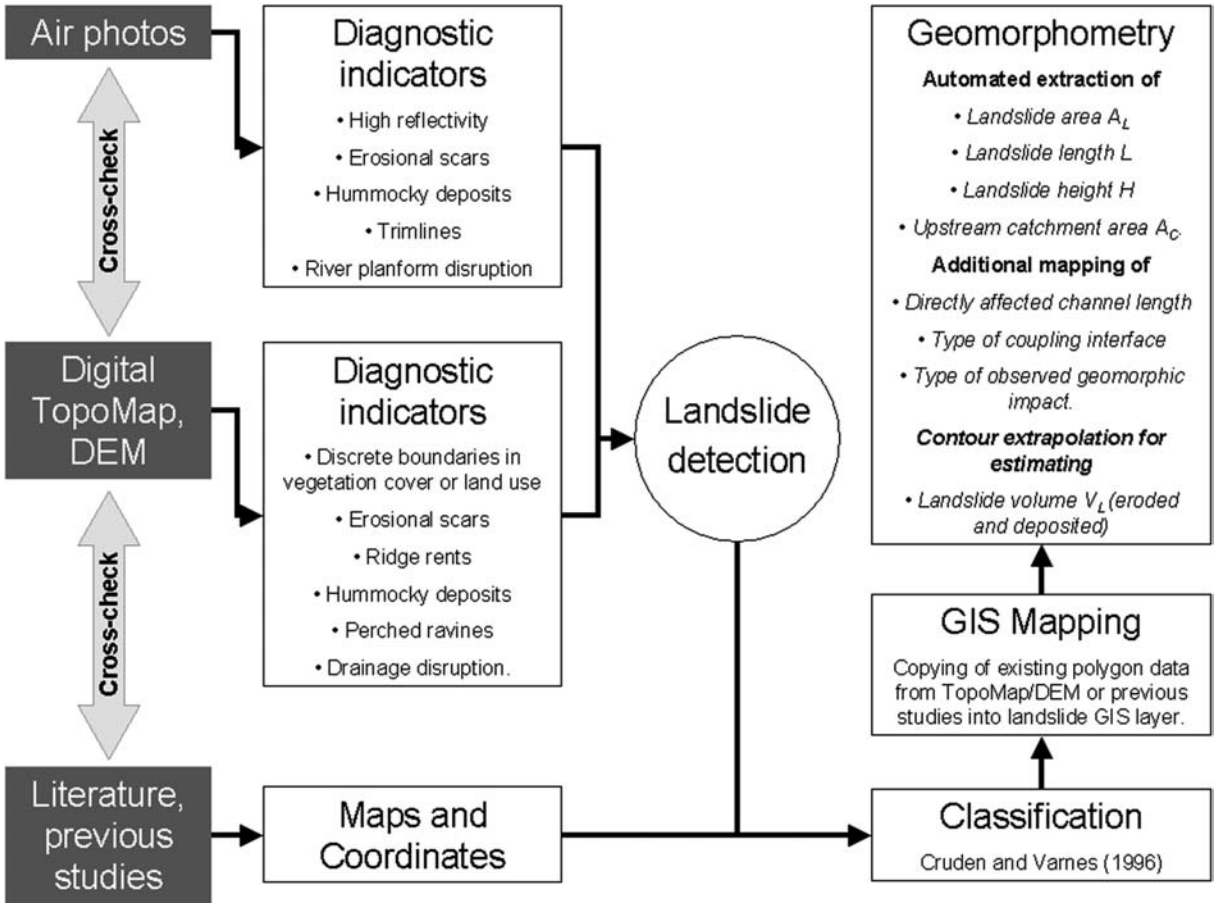

Fig. 5 Flowchart delineating the methods of landslide data acquisition, storage, and GIS-based analysis for the inventory

observed failures per km², can be modelled by as a power–law function of A_L [m²], with a slope β'=–1.44, and an intercept k'=14766 (R^2=96%) for the whole distribution. Using a subsample of the landslide distribution with A_L above where a conspicuous "roll-over" (Hovius et al. 1997) is evident, reduces β to –1.55, while not significantly improving the model fit (Fig. 7b). In other words, the number of mapped landslide occurrences per unit area is inversely related to their area, and the smaller landslides tend to be more numerous. Similar trends, including the roll-over at the lower end of the distribution, are commonly observed in landslide inventories (Malamud et al. 2004). The number of large landslides mapped per km² in the western Southern Alps is an order of magnitude greater than it is in Fiordland (Fig. 1a).

The ten largest slope failures affect up to several tens of km², and contribute to nearly 40% of the total area affected by landsliding A_{LT}. The largest of these—and one of the largest subaerial rock slide/avalanches on Earth—is the Green Lake rockslide (Hancox and Perrin 1994; Fig. 1a). It extends over 45 km², or 10% of A_{LT}, and has an estimated volume of 27 km³. Landslides with A_L>1 km² make up 83% of A_{LT}. Thus, A_{LT} in southwest New Zealand is clearly dominated by the largest events.

Some 7% of the landslides extend over >1,000 m vertically (Fig. 8b), while 20% have a runout L>1 km (Fig. 8c). Approximately two-thirds of the large landslides extend from ridge crest to valley floor, and some of them have dislocated ridge crests and interfluves, causing low-order stream piracy during or following the failure process. Most of the shallow and smaller failures extend over portions of the slope length only.

The slope angles of both scars and deposits combined of smaller (A_L<0.1 km²) landslides match the modal hillslope angle in the study area, and peak at φ_{mod}~39° (Fig. 2). This modal slope angle is also characteristic of hillslopes with dense montane forest cover. Given the dominance of large landslides by area, the slope-angle distributions for the large and the total number of landslides are similar. Large landslides show subdued topography with φ_{mod}~30° in the western Southern Alps, and ~23° in Fiordland (Fig. 2). In Fiordland, 64% of the terrain affected by large landslide exhibits φ_{mod}<30°. In the Southern Alps 54% of the landslide areas have φ_{mod} between 23° and 39°. There appears to be no preferential slope aspect for landsliding in Fiordland, when compared to the general and area-normalized distribution of slope aspect for hillslopes in the study area (Fig. 9). In the Southern Alps, however, significantly more landslides occur on SW-exposed slopes, while NE slopes appear to be more stable (Fig. 9).

About two third of the recorded smaller landslides are interpreted as rapid debris/rock slides and debris flows (in New Zealand also termed "debris avalanches"; Basher et al. 1988). These failures involve relatively small volumes (V_L<10⁴ m³), which strip hillslopes of vegetation and colluvium, leaving characteristic long, narrow scars. Large landslides are interpreted to

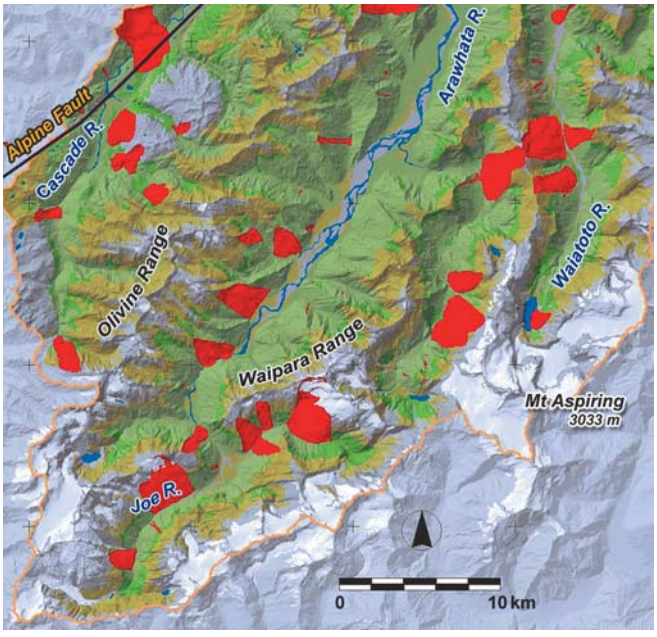

Fig. 6 Detail from the landslide inventory, highlighting mainly large (A_L>1 km^2) failures (*red*) in the heavily forested (*green*) upper Cascade, Arawhata, and Waiatoto catchments, western Southern Alps. *Yellow* and *grey-white shades* indicate subalpine tussock and bare alpine areas, respectively. Many of the failures appear to be still active or dormant

involve complex deep-seated rotational rock slides, structurally-controlled rockslide-wedge failures, and rock avalanches. There is also evidence of large-scale rock flow (Cruden and Varnes 1996) or sliding complexes of rock-mass creep in pelitic schist (Craw et al. 2003), associated with ridge rents and counterscarps (Beck 1968), toe-slope bulging, or valley-floor occlusion (Korup 2005).

The failure ages of many of the small debris slides and debris flows in the montane zone can be bracketed by comparison of air photos from successive time slices (Hovius et al. 1997). This is however not possible for the larger landslides, although historic records show that some major failures occurred during the twentieth century (Table 1). Mature forest covers 48% by area of the large landslide deposits, indicating a pre-historic (i.e. pre-1840) formation and/or reactivation age. Some of the larger failures exhibit glacial trimming, and may be of Holocene or older age.

Discussion

Analysis of 778 landslides in a medium-scale inventory covering southwest New Zealand shows that landslide area A_L ranges over three orders of magnitude. Frequency density, i.e. the observed number of landslide per unit area, can be modelled with a power–law function of A_L. The distribution shows that a small number of large landslides, which represent 10% of all failures, constitutes 83% of the total affected area. Similar magnitude–frequency relationships were reported from landslide inventories in different parts of the world (Malamud et al. 2004). Hovius et al. (1997) also noted the dominance of larger events in the spatio-temporal landslide distribution for the western Southern Alps.

The spatial pattern of landsliding and its magnitude–frequency relationship observed at present is biased however by (a) the unknown length of the observation period, and (b) the unknown role of high-intensity triggers such as earthquakes for regional landsliding episodes. While smaller failures tend indeed to be more frequent in historic times than larger ones (Table 1 lists the largest historically recorded landslides in the study area), their geomorphic evidence is eradicated by vegetation re-growth within <100 years (Hovius et al. 1997). Using API, their historic occurrence can be assumed to be documented rather completely.

Landslide preservation however is biased by size, and the deposits from larger slope failures should be geomorphologically recognisable for longer periods of time. Many of the landslides with estimated V_L>10^8 m^3 are still readily detectable in southwest New Zealand (Hancox et al. 2003), and the Green Lake rockslide deposit has survived the Holocene without much erosion. Thus, although such large and often deep-seated failures are assumed to occur less frequently than smaller ones, some elements of their morphological imprint on alpine relief have the potential to persist in the landscape for considerable periods of time, say 10^2–10^4 years. However, in the case of large failures in narrow or high-

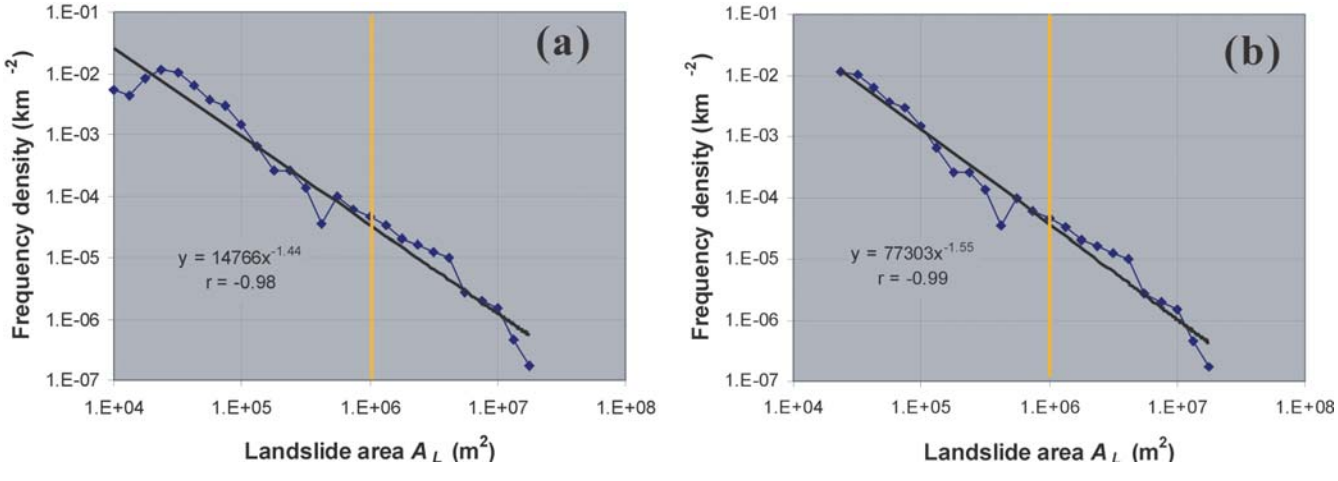

Fig. 7 Area-normalized frequency density (mapped landslides per km^2) as a function to landslide area A_L, for **a** n=778 landslides in the inventory, and **b** a sub-sample truncated at the "roll-over" at A_L~10$^{4.5}$ m^2. Frequency density can be modelled as a power–law function of A_L with slopes $ß$=–1.44 and –1.55, respectively

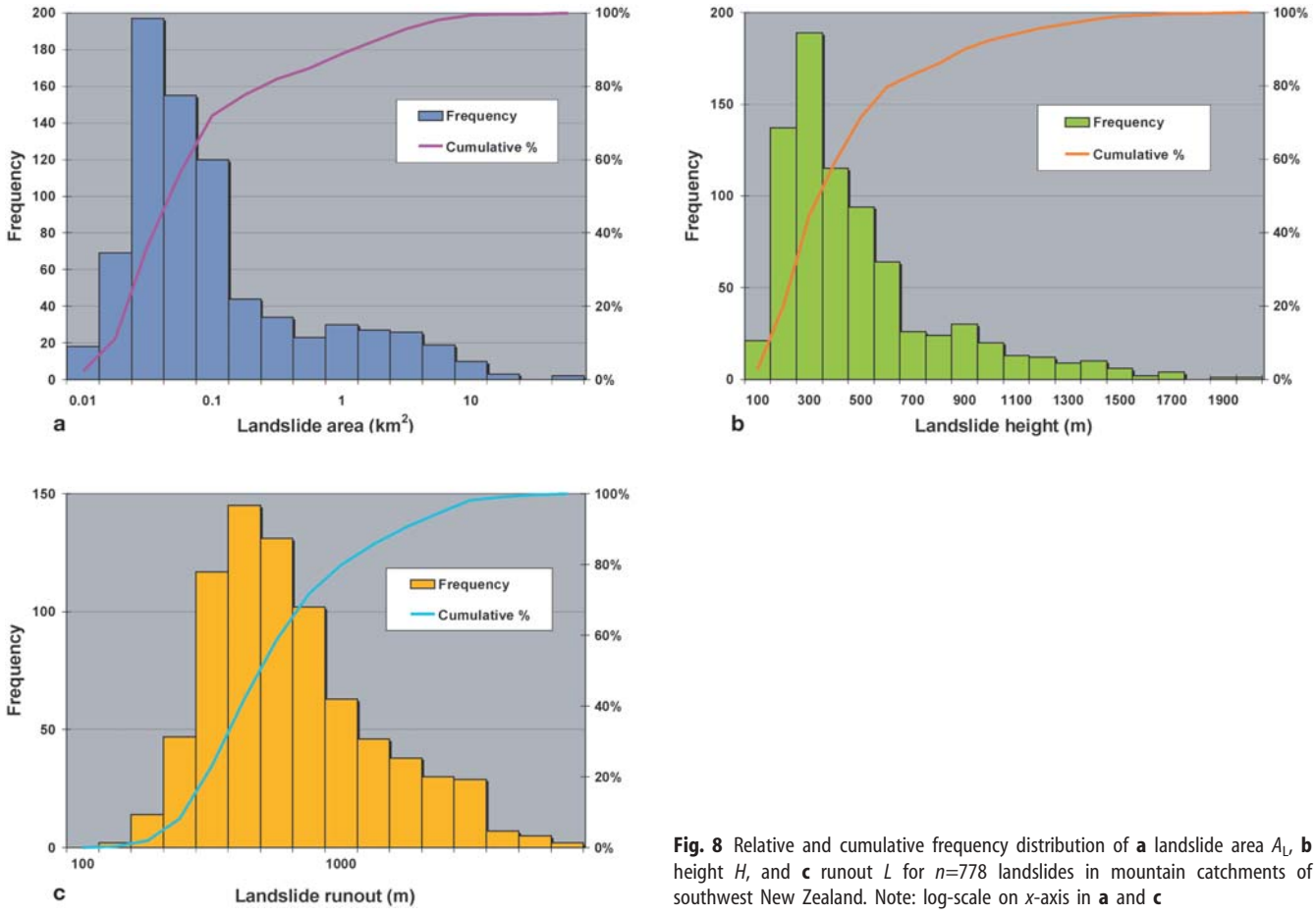

Fig. 8 Relative and cumulative frequency distribution of **a** landslide area A_L, **b** height H, and **c** runout L for n=778 landslides in mountain catchments of southwest New Zealand. Note: log-scale on x-axis in **a** and **c**

relief valleys, it is equally possible that evidence of the failures, particularly their debris, may be removed by the trunk river within a relatively short period, thus removing the potential for identifying the occurrence of the failure (Hancox et al. 1999; Korup et al. 2004).

Therefore, the amount of both small and large landslide deposits completely eroded since the emplacement of the oldest landslide in the sample, is unknown. Extrapolation of existing magnitude–frequency relationships such as the one proposed by Hovius et al. (1997) for the spatio-temporal occurrence of small shallow landslides in the western Southern Alps, toward the large-area "tail" of landslide distributions, is thus not possible. In a sense, such empirical predictions may not even be useful, given the potential for widespread coseismic and deep-seated landsliding during the next M~8 Alpine Fault earthquake (Wells et al. 1999). In other words, the occurrence of large landsliding may be controlled—to a degree hitherto unquantified—by episodic regional-scale seismic triggers. The current picture of slope instability in the region may thus represent a stage of geomorphic adjustment to high-intensity landsliding episodes. Finally, assuming recurrence intervals of M~8 earthquakes along the Alpine Fault every 250–300 years (Wells et al. 1999) throughout the Holocene, some of the older landslides would further have experienced several times of high-magnitude seismic ground shaking and possible reactivation. Such multiple or successive failures at the same site are difficult to represent in, and interpret from, the landslide inventory.

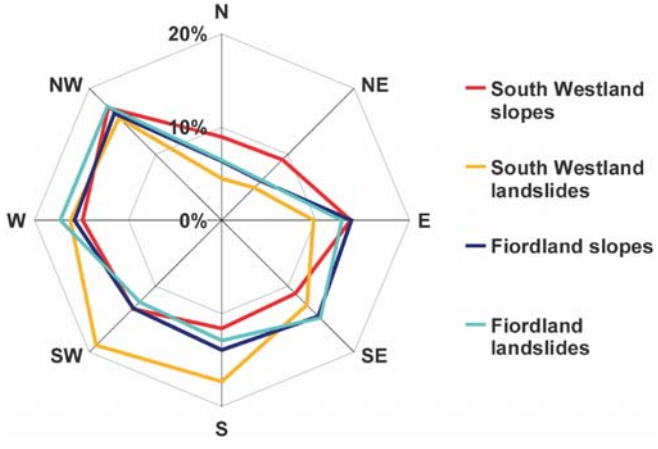

Fig. 9 Aspects of landslide-affected areas (scarps and deposits combined) and slope aspect, normalized by area, in the western Southern Alps (South Westland) and Fiordland

Modal surface angles of smaller and more numerous (A_L<0.1 km²) coincide with those of the hillslopes (φ_{mod}~39°; Fig. 2). This match can be interpreted as a direct result of frequent landsliding, assuming that the more numerous, small landslides occur on a much more frequent basis than the large landslides. In other words, hillslope have adjusted in the long-term to the frequent mechanism of shallow landsliding as a dominant geomor-

Table 2 Examples of large (A_L>1 km^2) landslides and their relation to catchment total sediment production from smaller failures in the western Southern Alps

Location	Catchment	Date	Landslide type	Volume (10^6 m^3)	Area (km^2)	Equivalent catchment-wide debris production from shallow landslides (year)[a]	Reference
Urquart Knob	Waitaha	Unknown	Rock-block slide	335	3.0	197	This study
Carls Ridge	Wanganui	Post-1960s	Complex rock-block slide	8	0.8	4	Korup and Crozier (2002)
Range Front	Wanganui	Unknown	?Rock avalanche	17.5	>1.1	8	Korup (2004)
Devastation Creek	Wanganui	Unknown	Complex	240	>2.1	114	Korup (2005)
Beelzebub Glacier	Adams	Post-1965	Rock avalanche	1.5	0.2	0.7	Korup (2005)
Mt Adams	Poerua	6 Oct 1999	Rock avalanche	10–15	1.6	8–12	Hancox et al. (1999)
Whymper Glacier	Whataroa	Unknown	Complex	4.5	0.5	4	This study
Undercite Creek	Fox	Jan 1994	Rock/debris slide	1–1.3	?	1–2	DTEC Consulting Ltd (2002)
Douglas A	Karangarua	Unknown	Rock slide (wedge failure)	14	0.8	11	Korup (2005)
Misty Peak[b]	Karangarua	Pre-1850	Complex rotational rock slide	800	6.7	615	Korup (2005), Fig. 10
Coleridge Creek	Karangarua	Pre-1850	Complex rotational rock slide	62	1.7	48	Korup and Crozier (2002)
Jumbo Creek	Makawhio	Unknown	Complex, sackung	240	3.5	218	This study (Fig. 4)

[a] Based on data from Hovius et al. (1997)
[b] Multiple failures likely

phic process in the area. However smaller failures do not achieve comparable reduction of slope angles. This is not surprising, given that most of these small-scale failures are assumed to be shallow—often translational—debris slides and debris flows, which mainly remove debris and vegetation mats from the slopes. Rapid entrainment of this debris by surface runoff and rivers allows the maintenance of the characteristic modal slope angle without creating major debris accumulations. On the hillslope scale, many of these debris failures are thus superimposed on the existing relief, hence the coincidence in modal slope angles. In contrast, large failures cause much more widespread destruction of local relief and forming of low-gradient slopes (Fig. 4). Significantly larger portions of hillslopes experience re-shaping and lowering of gradients well below 39° through deep-seated rotational large landslides or rock flow (Figs. 2 and 4).

The geomorphic significance of the preserved large landslide deposits in southwest New Zealand is highlighted when comparing their volumes with estimated rates of sediment production from historic shallow landsliding. The total catchment production of debris from shallow landslides with A_L<1 km^2 is estimated at $1.2\pm0.5\times10^6$ m^3/year ($\pm1\sigma$) for 13 catchments in the western Southern Alps (Hovius et al. 1997). Empirical volume–area relationships show that large deep-seated landslides entrain >10^6 m^3 of material. Thus in a single event they can produce 10^0–10^2 years worth of sediment generated from smaller failures in the same catchment (Table 2).

The deposit volume of a complex rotational rockslide at Misty Peak, Karangarua River, for example (Fig. 10), is $V_L\sim800\times10^6$ m^3 and equates to >600 years of sediment produced from catchment-wide shallow landsliding. The same deposit volume corresponds to 25 years of contemporary sediment yield from the western Southern Alps (62 Mt/year; Hicks et al. 2003). Such figures are first-order indications, and absolute dates on large landslides are

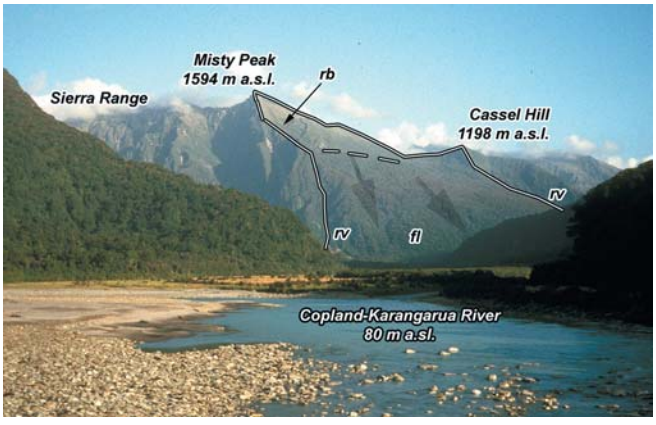

Fig. 10 Complex rotational rockslide below Misty Peak at the confluence of Copland and Karangarua Rivers, western Southern Alps. Failure extends over 6.7 km^2 and involves $\sim800\times10^6$ m^3 (Korup, 2005). Like many other large landslides in the area, the deposit is covered by dense forest; *rb* rotated blocks; *fl* flow lobes; *rv* perched ravines eroding lateral scarps of the landslide. *Dashed line* indicates upper limit of main deposit

needed for future research to assess the relative contribution of these large-scale sediment sources to total production over time. The preservation of large landslide deposits attests to locally high sediment sequestration despite extreme erosion rates. In many cases the deposits are simply too large to be eroded completely within 10^1–10^2 years, allowing the "survival" of prehistoric landslide accumulations. Yet do neither the size distribution or geomorphic evidence of landslide remnants allow quantifying the amount of landslide debris eroded since emplacement.

The findings of Hancox et al. (2003) support the notion of a dominance of larger events in landslide sediment production.

During the 2003 Fiordland earthquake, the largest 15 out of 422 mapped landslides produced ~90% of the total sediment (4.5–5.8×10^6 m^3). This is nearly an order of magnitude higher than the annual sediment yield from the Fiordland Mountains, which Hicks et al. (2003) estimated at 1.3 Mt. The deposit of the 13,000-year-old Green Lake rockslide (V_L=27 km^3; Hancox and Perrin 1994) would thus account for nearly 8,700 years of contemporary yield. Nonetheless, most of the deposit however has remained in situ. About 170×10^6 m^3 have been eroded from the deposit from what appears to be a breach channel. This corresponds to only 0.6% of the total displaced volume, yet would require average sediment discharge of 1.4×10^4 m^3/year, and a specific yield of 5.5×10^2 t/km^2/year. These rates are still relatively high for this region (Pickrill 1993), and illustrate the importance of better understanding large-scale slope failures in the context of both process dynamics and long-term landform evolution in mountain regions.

Conclusions

The size distribution of a new landslide inventory for the western Southern Alps and Fiordland Mountains shows a negative power–law relationship between spatial density of occurrence and landslide area A_L over three orders of magnitude. Although observed in other landslide studies (Malamud et al. 2004), this relationship is surprising, given the lack of absolute age constraints, and thus the temporal sampling interval encompassed by (a) the inventory in general, and (b) the larger failures, in particular. Given that the large landslide deposits (A_L>1 km^2, and V_L>10^6 m^3) identified represent geomorphic remnants of an unquantifiably larger population of postglacial slope failures, extrapolation of magnitude–frequency relationships toward the large-area "tail" of distributions is not possible. The amount of material contained in individual large landslide deposits preserved in the erosional mountain landscape of southwest New Zealand equates to 10^0–10^2 years worth of catchment-wide sediment production from shallow failures (Table 2). The residence time of some of these deposits is inferred to be between 10^2 and 10^4 years, and illustrates their geomorphic significance as temporary storage of large amounts of sediment in an erosional mountain landscape.

Acknowledgements

Thanks are due to the support and advice of Michael Crozier, and the constructive reviews by David Barrell, Timothy R. Davies, and Mauri McSaveney

References

Augustinus PC (1992) The influence of rock mass strength on glacial valley cross-profile morphometry: a case study from the Southern Alps, New Zealand. Earth Surf Process Landforms 17:39–51

Basher LR, Tonkin PJ, McSaveney MJ (1988) Geomorphic history of a rapidly uplifting area on a compressional plate boundary: Cropp River, New Zealand. Z Geomorphol NF 69:117–131

Beck AC (1968) Gravity faulting as a mechanism of topographic adjustment. N Z J Geol Geophys 11:191–199

Brardinoni F, Slaymaker O, Hassan MA (2003) Landslide inventory in a rugged forested watershed: a comparison between air-photo and field survey data. Geomorphology 54:179–196

Claypool AL, Klepeis KA, Dockrill B, Clarke GL, Zwingmann H, Tulloch A (2002) Structure and kinematics of oblique continental convergence in northern Fiordland, New Zealand. Tectonophysics 359:329–358

Craw D, Nelson E, Koons PO (2003) Structure and topographic evolution of the Main Divide in the Landsborough-Hopkins area of the Southern Alps, New Zealand. N Z J Geol Geophys 46:553–562

Cruden DM, Varnes DJ (1996) Landslide types and processes. In: Turner AK, Schuster RL (eds) Landslides, investigation and mitigation. Special Report 247, Transportation Research Board, National Research Council, Washington, DC, pp 36–75

Dai FC, Lee CF (2001) Frequency–volume relation and prediction of rainfall-induced landslides. Eng Geol 59:253–266

DTEC Consulting Ltd (2002) West Coast Regional Council: natural hazards review. http://www.wcrc.govt.nz/environment/west_coast_natural_hazards.htm

Guzzetti F, Malamud BD, Turcotte DL, Reichenbach P (2002) Power–law correlations of landslide areas in central Italy. Earth Planet Sci Lett 195:169–183

Hancox GT, Perrin ND (1994) Green Lake landslide: a very large ancient rock slide in Fiordland, New Zealand. In: Oliveira R, Rodrigues LF, Ceolho AG, Cunha AP (eds) Proceedings of the seventh international congress of International Association of Engineering Geology, Lisboa, pp 1677–1689

Hancox GT, McSaveney MJ, Davies TR, Hodgson K (1999) Mt. Adams rock avalanche of 6 October 1999 and subsequent formation and breaching of a large landslide dam in Poerua River, Westland, New Zealand. Institute of Geological and Nuclear Sciences Science Report 99/19, Lower Hutt

Hancox GT, Cox SC, Turnbull IM, Crozier MJ (2003) Reconnaissance studies of landslides and other ground damage caused by the M_w 7.2 Fiordland earthquake of 22 August 2003. Institute of Geological and Nuclear Sciences Science Report 2003/30, Lower Hutt

Henderson RD, Thompson SM (1999) Extreme rainfalls in the Southern Alps of New Zealand. J Hydrol (N Z) 38:309–330

Hicks M, Shankar U, McKerchar A (2003) Sediment yield estimates: a GIS tool. NIWA Water Atmos 11:26–27

Hovius N, Stark CP, Allen PA (1997) Sediment flux from a mountain belt derived from landslide mapping. Geology 25:231–234

Kim KJ, Sutherland R (2004) Uplift rate and landscape development in southwest Fiordland, New Zealand, determined using ^{10}Be and ^{26}Al exposure dating of marine terraces. Geochim Cosmochim Acta 68:2313–2319

Korup O (2004) Geomorphic implications of fault zone weakening: slope instability along the Alpine Fault, South Westland to Fiordland. N Z J Geol Geophys 47:257–267

Korup O (2005) Large landslides and their effect on sediment flux in South Westland, New Zealand. Earth Surf Process Landforms (in press)

Korup O, Crozier M (2002) Landslide types and geomorphic impact on river channels, Southern Alps, New Zealand. In: Rybar J, Stemberk J, Wagner P (eds) Proceedings of the first European conference on landslides, Prague, pp 233–238

Korup O, McSaveney MJ, Davies TRH (2004) Sediment generation and delivery from large historic landslides in the Southern Alps, New Zealand. Geomorphology 61:189–207

Land Information New Zealand (2002) NZTopoOnline Digital Internet Map Server (IMS). Crown copyright reserved. http://www.topoonline.linz.govt.nz

Malamud BD, Turcotte DL, Guzzetti F, Reichenbach P (2004) Landslide inventories and their statistical properties. Earth Surf Process Landforms 29:687–711

Mark AF (1998) Te Waahipounamu: south-west New Zealand World Heritage Area. Ecological research and conservation history. J R Soc N Z 28:657–684

Norris RJ, Cooper AF (2000) Late Quaternary slip rates and slip partitioning on the Alpine Fault, New Zealand. J Struct Geol 23:507–520

Perrin ND, Hancox GT (1992) Landslide-dammed lakes in New Zealand. Preliminary studies on their distribution, causes and effects. In: Bell DH (ed) Landslides. Glissements de terrain. Balkema, Rotterdam, pp 1457–1466

Pickrill RA (1993) Sediment yields in Fiordland. J Hydrol (N Z) 31:39–55

Terralink New Zealand Ltd (2000) New Zealand land cover. Digital polygon-based land cover data from SPOT satellite coverage 1994–1996, positional accuracy ±25 m, minimum mapping unit 0.01 km^2, classification accuracy 90%, Wellington

Thomson R (1994) The 1984 Iris Burn Slip: a geological appraisal. Institute of Geological and Nuclear Sciences Science Report 94/38, Lower Hutt

Wells A, Duncan RP, Stewart GH, Yetton MD (1999) Prehistoric dates of the most recent Alpine Fault earthquakes, New Zealand. Geology 27:995–998

Wratt DS, Revell MJ, Sinclair MR, Gray WR, Henderson RD, Chater AM (2000) Relationships between air mass properties and mesoscale rainfall in New Zealand's Southern Alps. Atmos Res 52:261–282

O. Korup (✉)
WSL Swiss Federal Institute for Snow and Avalanche Research SLF,
Flüelastr. 11, 7260 Davos, Switzerland
e-mail: korup@slf.ch
Tel.: +41-81-4170354
Fax: +41-81-4170110